



CHEMICAL SCIENCES

TiO₂ nanotube arrays with visible light catalytic

ENYANG LIU & XIAOJIAN BI

Abstract: The TiO₂ nanotube arrays were prepared by anodization, and the crystal structure was changed by calcination at different temperatures. The photocatalytic performance of the samples was measured by the degradation of rhodamine B under visible light. The TiO₂ nanotubes calcined at 600 °C showed higher photocatalytic activity than other samples. The prepared catalyst is characterized by a variety of techniques, including X-ray diffraction, scanning electron microscopy, ultraviolet-visible diffuse reflectance spectroscopy, Raman, photoluminescence spectroscopy and electrochemical testing. The reasons for improving the catalytic activity were studied from the aspects of crystal structure, surface morphology, and photoelectric properties, and the catalytic mechanism was studied. The results show that the TiO₂ nanotubes calcined at 600°C contain two phases of anatase and rutile. Compared with pure phase TiO₂, the charge transfer resistance is reduced and the electron-hole reorganization is well suppressed. In addition, it affects the band structure and improves the absorption of visible light. At the same time, studies have found that the main active substances in the catalytic process are h⁺ and ·OH.

Key words: TiO₂ nanotube arrays, rhodamine B, anatase; rutile, active substances.

INTRODUCTION

The study found that TiO₂ semiconductor is an n-type semiconductor, which is widely used in gas sensors (Sun et al. 2019, Duy et al. 2008, Morris et al. 2001), solar cells (Liu et al. 2018, Fitra et al. 2013, Adawiya et al. 2017) and photocatalysis (Tieng et al. 2011, Pham et al. 2016, Gao et al. 2014) because of its non-toxicity, low cost, high activity and good stability. However, TiO₂ also suffers from a limited photocatalytic application due to its weak adsorptive property, easy aggregation and recycling problems which would cause the secondary pollution after degradation process. The researchers used different methods to change the morphology, particle size and crystal phase of TiO₂ to improve its photocatalytic activity (Chiarello et al. 2005). At present, the preparation methods of TiO₂ mainly include hydrothermal method (Sugimoto et al. 2002),

anodic oxidation (Liang et al. 2011), flame spray pyrolysis (Macak et al. 2007, Mohamed & Rohani 2011) and sol-gel method (Hwang et al. 2013). Among these the TiO₂ nanotube arrays (TNTs) prepared by the anodic oxidation method is likely to recover, not easy to agglomerate, and has no secondary pollution. And compared to nanoparticles, vertically oriented structures of TNTs provide especially high energy conversion efficiencies by providing direct electron diffusion pathways at interfaces.

Although these advances, the photocatalytic efficiency of TNTs is still greatly limited due to its wide band gap and high photo-generated electron-hole recombination rate (Zeng et al. 2015). In order to reduce the band gap and improve the visible light catalytic activity, the predecessors improved the catalytic performance of TiO₂ by changing the crystal

form (Qian et al. 2018, Ghayeb & Ghonchehi 2015), metal ion doping (Tian et al. 2009, Choi et al. 2016), semiconductor composite (Li et al. 2013, Qamar et al. 2015) and noble metal deposition (Wang et al. 2015). Among the many methods, it is much simpler to change the crystal phase structure. TiO₂ has three crystal forms of anatase, rutile and brookite. The photocatalytic effects of different crystal types are particularly different, and the composite materials of different crystal phases have better photocatalytic activity (Barnard & Curtiss 2005, Dicesare & Lakowicz 2001, Wiley et al. 2001). Thus, predecessors have done a lot of research in this area. Aref Mamakhel et al. (2013) used hydrothermal method to synthesize a single rutile nanometer TiO₂ with a particle size of less than 10 nm, which provided a new method for obtaining rutile TiO₂ at low temperature. Zhang et al. (2009) has synthesized an anatase TiO₂ single crystal photocatalyst with high activity by microwave-assisted hydrothermal method. Li et al. (2017) prepared g-C₃N₄/rutile TiO₂ and g-C₃N₄/brookite TiO₂ composites by a simple solvothermal method, and studied the effect of rutile phase TiO₂ and brookite TiO₂ on the photocatalytic activity of g-C₃N₄. Mi et al. (2012) studied the formation mechanism and crystal growth of TiO₂ in high temperature and high pressure fluid. When HCl is used as an additive, pure rutile TiO₂ nanoparticles can be formed, while using H₂SO₄ can obtain pure anatase TiO₂. According to previous studies, there are few studies on the preparation of TiO₂ with different crystal phases on the titanium mesh by anodization.

In this research, simple anodic oxidation method was used to prepare amorphous TNTs. The TNTs crystal phase was changed by calcination at different temperatures, and the effect of different crystalline TNTs on the photocatalytic activity was investigated. In

experiment, titanium mesh is used as the matrix, but titanium does not participate in the catalysis, so it will not interfere with the results of the catalysis. Since the TNTs uniformly cover the substrate and the titanium has not yet entered the TiO₂ lattice, it will not form a heterostructure with TNTs.

MATERIALS AND METHODS

Materials

The raw materials used include hydrofluoric acid (HF, 40.0%, CAS: 7664-39-3), nitric acid (HNO₃, 65.0-68.0%, CAS: 7697-37-2), isopropanol (C₂H₆OH, 99.7%, CAS: 67-63-0) and titanium mesh (99%). All raw materials were purchased from Sinopharm Chemical Reagent Network without further purification.

Synthesis

Before anodization, the titanium mesh (2×4 cm) was sequentially sonicated in acetone and pure ethanol for 15 min, followed by etching in a mixture of HF/HNO₃/H₂O (1:4:5 in volume) for 30 s to remove the oil and oxide layer on the surface, rinsing with deionized water, and drying under flowing N₂. The titanium mesh after the above treatment is used as the anode, and the graphite plate is the cathode (2×4 cm). The electrolyte is an aqueous solution containing 1 % HF. Anodization was performed at 15 V for 1 hour, then washed with deionized water and dried. Under a protective atmosphere of argon gas, the obtained sample was calcined for 2 h in a tube furnace, and the calcining temperatures were 300 °C, 400 °C, 500 °C, 600 °C, and 700 °C (heating rates of 5°C/min), respectively.

Catalyst characterizations

The crystal phase structure of the sample was determined using an X'Pert PRO MRD type X-ray diffractometer. The SEM was performed using

a JSM-7200 field emission scanning electron microscope. The PL spectrum was measured with a F-7000 type fluorescence spectrophotometer, using a Xe lamp (excitation wavelength is 365 nm) as light source. The DRS spectrum was measured using a U-3900 UV-Vis spectrophotometer and BaSO₄ was used as the reference sample.

Photocurrent response (PR) tests were performed using a CS130 electrochemical workstation. A three-electrode system was used, and the corresponding three electrodes are a working electrode, a reference electrode (Ag/AgCl saturated KCl), and a counter electrode (Pt rod). The titanium mesh was cut into 1 cm×1.5 cm, and the anodized area was 1 cm². An alternating current voltage of 10 mV was applied, and the initial potential was 0 V. The photocurrent response diagram was measured using a 350 W Xe lamp as the light source and an aqueous solution of Na₂SO₄ (0.3 M) as the electrolyte in the frequency range of 10⁵ Hz to 10⁻² Hz.

Photocatalytic reaction

The photocatalytic activities of TNTs were tested by RhB (10 mg/L) degradation under visible-light irradiation. The light source is a 250 W high-pressure mercury lamp (7.0 mW/cm²), and the wavelength below 420 nm is filtered by a filtering device. The photocatalytic performance of TNTs calcined at different temperatures was tested. Place a piece of titanium mesh in 75 ml of the prepared RhB solution for 20 min in the dark, and then transfer the solution to the light source for photodegradation reaction. After centrifuging all the catalyzed solutions twice, the supernatant was taken and the absorbance was measured at 554nm with a 752 spectrophotometer. The sample was catalyzed several times to test its stability.

Mechanism exploration

In order to confirm the mechanism of this catalytic reaction, benzophenone (BQ), triethanolamine (TEOA) and tert-butanol (TBA) were used as scavengers for superoxide radicals (O₂⁻), holes (h⁺) and hydroxyl radicals (·OH). These three kinds of scavengers (0.01 mol/L) were added to three same RhB solutions respectively before dark adsorption, and the rest of the process was consistent with the degradation experiment (Hong et al. 2016).

RESULTS AND DISCUSSION

XRD analysis

All samples were checked using XRD to determine the crystal phase structure of the TNTs material (Figure 1). The XRD pattern of the titanium mesh is the peak of pure titanium without any other impurities. The titanium mesh after anodization does not show the peak of TiO₂, but it shows the peak of TiO₂ after calcination under the protection of argon atmosphere, which can indicate that TiO₂ can be prepared by anodization, and the TiO₂ is amorphous state. The samples after calcination at 300 °C, 400 °C and 500 °C all shows anatase-type TiO₂ peaks. The two main diffraction peaks are located at 2θ

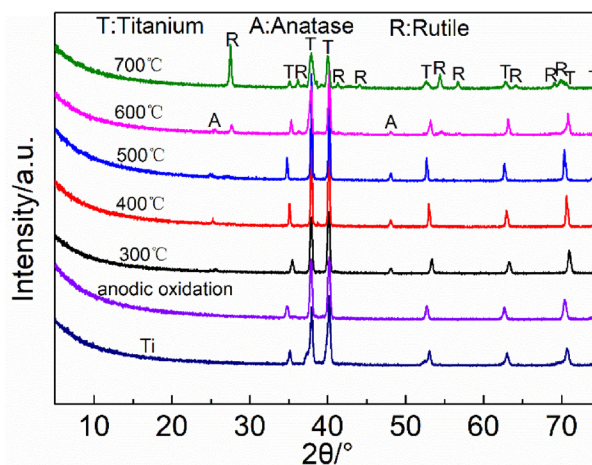


Figure 1. XRD patterns of TNTs calcined at different temperatures.

of 25.28 ° and 48.05 °, which correspond to the characteristic peaks of the anatase phase (101) and (200) crystal planes, respectively. And the peak strength increases slightly with increasing temperature, indicating that anatase TiO₂ has increased. The peak strength of the anatase-type TiO₂ of the sample calcined at 600 °C weakened, and a peak of rutile-type TiO₂ appeared. The diffraction peak of the sample calcined to 700 °C was completely transformed into rutile TiO₂. Diffraction peaks at 27.4°, 36.1°, 41.2°, 44.1°, 54.3°, 56.6°, 64.0°, 69.0° and 69.8° were observed in all cases, corresponding to the crystal faces of rutile TiO₂, which are (110), (101), (111), (210), (211), (220), (310), (301) and (112), respectively. It can be concluded from the above that TiO₂ was prepared after anodization, and the crystalline phase can be changed after roasting at different temperatures. With the increase of temperature, the crystalline phase of TiO₂ gradually changes from anatase to rutile.

Characterization of morphology and structure

SEM was performed to investigate the morphologies of the prepared samples (Figure 2). The TiO₂ prepared by anodizing is a tubular structure with a flat surface and uniform diameter, an inner diameter of about 100 nm, a wall thickness of about 8 nm and length is about 350 nm (Figure 2a). After calcining at 300 °C, 400 °C and 500 °C, the sample did not change the nanotube structure and the length has not changed significantly, but the wall thickness increased. The wall thickness of the nanotubes calcined at 500 °C could reach 15 nm (Figure 2b-d). After calcining at 600 °C, the wall thickness of nanotubes increased greatly and cracked severely, and only a small amount of nanotubes still maintained a tubular structure. The ruptured tube wall is spherically stacked (Figure 2e). However, almost all nanotubes were ruptured after calcination at 700 °C and

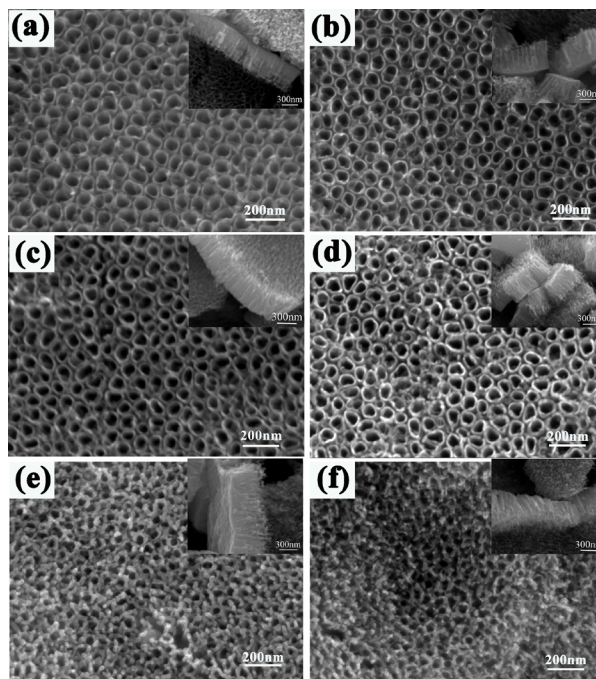


Figure 2. SEM images of (a) uncalcined TNTs and (b-f) 300 °C, 400 °C, 500 °C, 600 °C and 700 °C calcined TNTs.

the length also becomes shorter, about 310 nm (Figure 2f).

Raman spectroscopy

Raman scattering is more sensitive to the detection of the short-range structure of crystals, which makes it easier to research the crystal phase structure and quality of nano-sized crystals. The anatase TiO₂ nanocrystals have six Raman active modes ($A_{1g} + 2B_{1g} + 3E_g$), which are located at 145 cm⁻¹ [$E_g(1)$], 197 cm⁻¹ [$E_g(2)$], 399 cm⁻¹ [$B_{1g}(1)$], 513 cm⁻¹ [A_{1g}], 519 cm⁻¹ [$B_{1g}(2)$], and 639 cm⁻¹ [$E_g(3)$]. Four characteristic peaks were observed in the measured Raman spectrum (Figure 3), at 145 cm⁻¹, 399 cm⁻¹, 513 cm⁻¹, and 639 cm⁻¹. And rutile TiO₂ nanocrystals have four Raman active mode (A_{1g} , B_{1g} , B_{2g} , E_g), two characteristic peaks of 443 cm⁻¹ (E_g) and 610 cm⁻¹ (A_{1g}) were observed. The broad peak at 232 cm⁻¹ is a composite peak and a characteristic Raman peak of rutile TiO₂. The samples calcined at 300 °C, 400 °C and 500 °C are anatase TiO₂, and there is no rutile

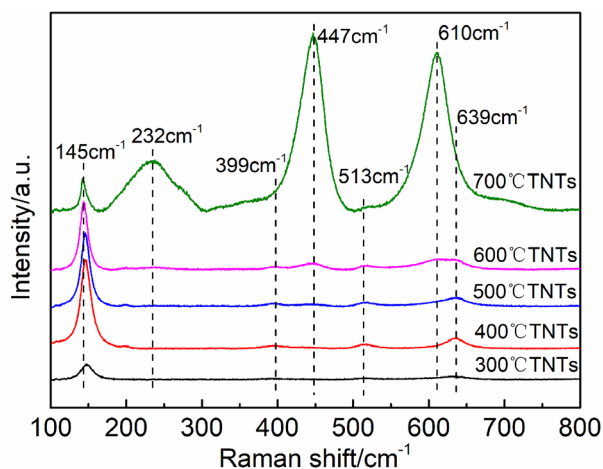


Figure 3. Raman spectra of TNTs.

Raman peak. As the temperature rises to 500°C the characteristic peak of anatase increases. The sample calcined at 600°C began to show the characteristic peak of rutile TiO₂, but the characteristic peak of corresponding anatase TiO₂ still exists, so it is a mixed crystal form of anatase and rutile. After calcination at 700°C, only a small amount of anatase TiO₂ is present in the sample.

Photoluminescence spectroscopy

The recombination ratio of electron-hole pairs is an important factor for measuring the performance of photocatalysts. The photoluminescence spectra (Figure 4) of the samples were tested to compare the recombination ratios of electron-hole pairs of TNTs baked at different temperatures. Generally, the lower the fluorescence intensity, the lower the recombination efficiency of the photoinduced electron-hole pair, and therefore the higher the photocatalytic activity. Figure 4 shows the PL spectral excitation wavelength at 365 nm. The PL spectra of TNTs exhibits a strong emission band centered at about 440 nm, which was attributed to the recombination process of self-trapped excitations (Luo et al. 2015, Tonda et al. 2015). Obviously, the PL strength of uncalcined TNTs is significantly higher than that

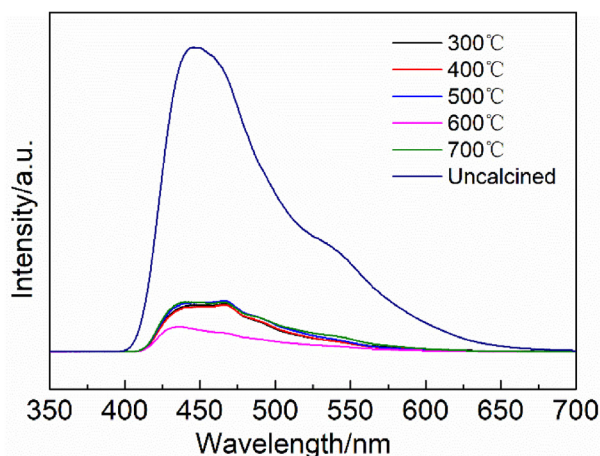


Figure 4. PL spectra of TNTs calcined at different temperatures.

of TNTs treated at high temperature, indicating amorphous TNTs has the highest electron-hole pair recombination rate, which reduces the photodegradation efficiency. The fluorescence intensity of the calcined TiO₂ material is greatly suppressed. The fluorescence quenching degree of TiO₂ calcined at 300 °C, 400 °C, 500 °C and 700 °C is almost the same. However, the strength was especially reduced after firing at 600 °C. The results show that the recombination efficiency of electron-hole pairs of TiO₂ composites containing both anatase and rutile phases is much lower than that of single crystal phase of TNTs.

Electrochemical test

In order to further verify the conclusions obtained from the PL spectrum, a transient photocurrent response was further performed on the sample (Figure 5). It can be seen that uncalcined TNTs can be excited in visible light, but the photocurrent response is weak, indicating that the inferior photocatalytic activity. After calcination, TNTs can be strongly excited in visible light, and the photocurrent response is particularly enhanced. As the temperature increases, the photocurrent response increases first and then decreases. The TNTs calcined at 600 °C have the strongest

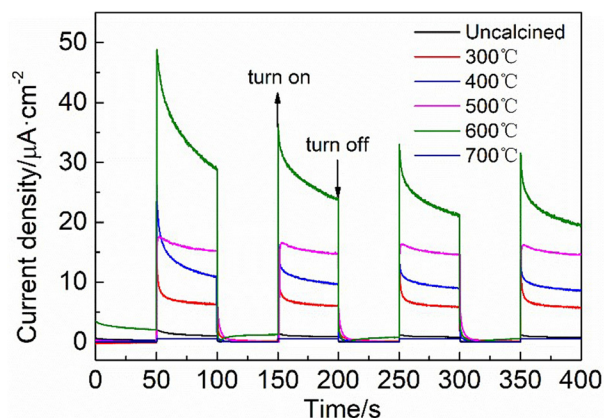


Figure 5. transient photocurrent responses of TNTs calcined at different temperatures.

response to visible light, indicating that TNTs with a certain proportion of anatase and rutile mixed phase have the highest photocatalytic activity. This is consistent with the results obtained with the PL spectrum.

Optical performance studies

The UV-vis DRS of TNTs calcined at different temperatures is shown in Figure 6a. Pure TiO₂ nanotube arrays showed strong light absorption in the ultraviolet region below 385 nm and showed weak light absorption in the wavelength range of 400–600 nm, which is due to light scattering caused by cracks or pores in the nanotube arrays (Zhang et al. 2015). In contrast, the absorption performance of the samples after calcination in the visible light range of 550 nm–800 nm was significantly improved. The samples calcined at 300 °C, 400 °C, and 500 °C were red-shifted compared to the non-calcined samples, which also showed that the absorption of visible light was improved. After sintering at 600 °C, the sample has a strong absorption of visible light, indicating the TNTs of two mixed crystal phases effectively improves the light absorption capacity. Due to the different Fermi energy levels of the two crystalline forms of TiO₂ (Bickley et al. 1991), a potential barrier can be created between the two-phase interfaces, which can

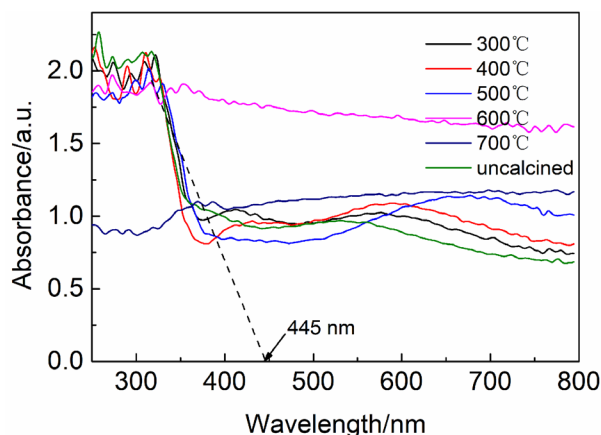


Figure 6. UV-vis spectra of TNTs calcined at different temperatures.

promote the transfer, separation and migration of electrons and holes to the surface of the catalyst, all of which greatly enhance the visible light absorption performance. However, the samples after calcining at 700 °C did not improve the visible light absorption performance, but greatly reduced the ultraviolet light absorption performance, indicating that the single rutile TiO₂ has a poor response to ultraviolet-visible light. In addition, it can be seen from the figure that the absorption edges of the uncalcined TNTs, 500 °C TNTs and 600 °C TNTs are 412 nm, 426 nm and 445 nm, respectively. Substitute the wavelength corresponding to the absorption edge into the formula $E_g(\text{eV})=1240/\lambda(\text{nm})$ (Feng et al. 2018, Wu et al. 2019). The calculated band gaps of the samples are 3.06 eV, 2.91 eV and 2.78 eV, respectively. This also explains that the TNTs calcined at 600 °C have better light absorption properties than other samples.

Catalytic performance evaluation

The photocatalytic activity of TNTs calcined at different temperatures was measured by the degradation of RhB under visible light. Figure 7a-g are absorption spectra of RhB at different times during catalytic degradation. In the absorption spectrum of the degraded RhB of the

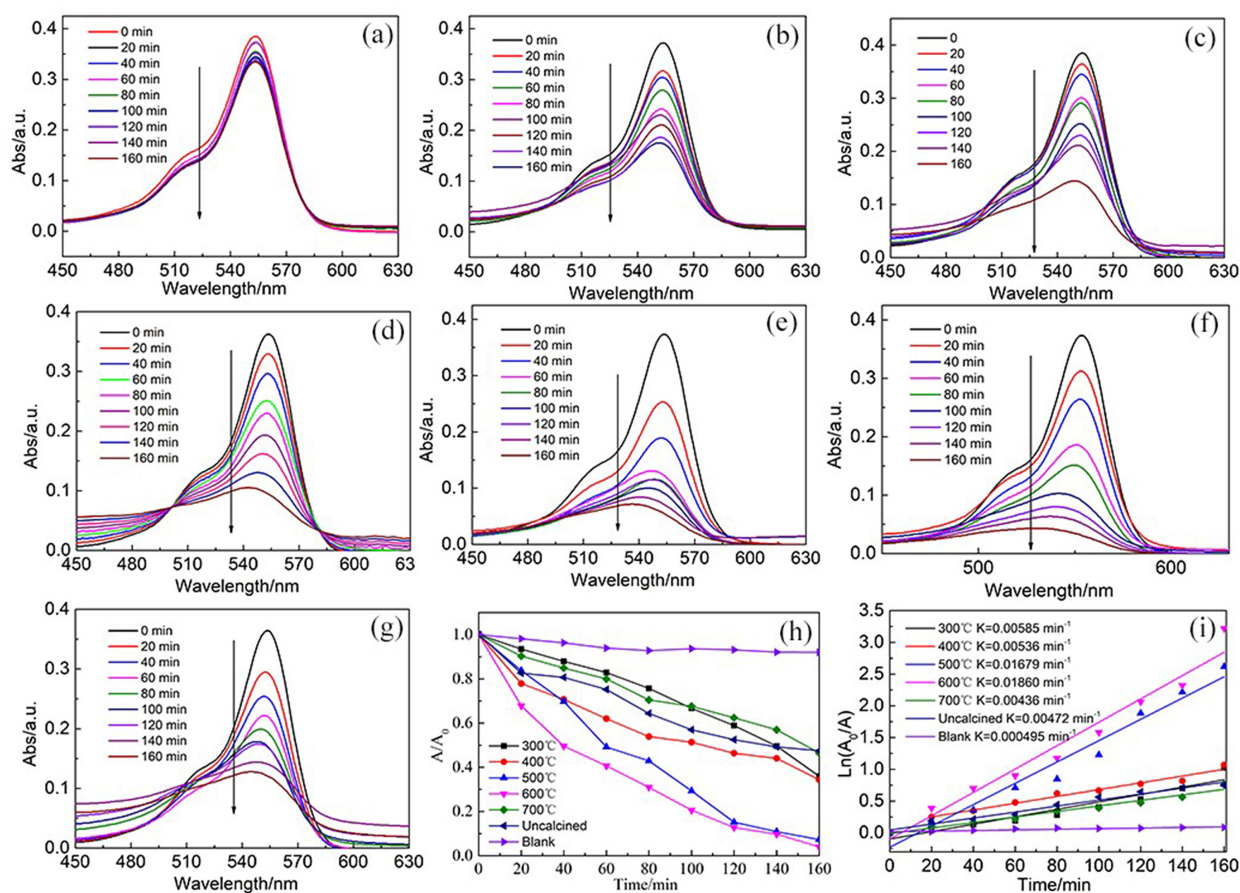


Figure 7. UV-Vis absorption spectra of photocatalytic RhB degradation over (a) blank, (b) uncalcined TNTs, (c) 300 °C TNTs, (d) 400 °C TNTs, (e) 500 °C TNTs, (f) 600 °C TNTs, (g) 700 °C TNTs, (h) photodegradation efficiency toward RhB measured at 554 nm and (i) the photocatalytic rate curves and corresponding fitted kinetics curves.

blank sample, it can be seen that RhB is basically not degraded, and its maximum absorption wavelength is 554 nm (Figure 7a). Figure 7b-g shows that all TNTs samples do not have much influence on the absorption wavelength of RhB. Compared with uncalcined TNTs, the degradation rate of RhB by TNTs after heat treatment is greatly increased. With the increase of heat treatment temperature, the degradation rate first increases and then decreases and the sample calcined at 600 °C has the best catalytic effect. It can be seen from the Figure 7h that the direct degradation of RhB can be neglected (<5%). Uncalcined TNTs also has degradability, and the final degradation rate can only reach 52.5%. However, the catalytic effect of TNTs calcined at 300 °C and 400 °C was

not significantly enhanced, probably because there was only a small amount of anatase TiO₂. After 500 °C calcination, the catalytic effect was greatly enhanced, and finally reached 92.7%. And after calcination at 600 °C, the degradation rate is further increased, and can finally reach 96%. The results show that the TNTs mixed with anatase and rutile has the best catalytic effect and the highest photocatalytic activity. It shows that TNTs with a certain proportion of anatase and rutile have the best catalytic effect and the highest photocatalytic activity. The photocatalytic degradation rate of TNTs calcined at 700 °C decreased obviously, indicating that the single rutile TNTs has low catalytic activity and is lower than that of single anatase. The

photocatalytic degradation rate of TNTs calcined at 700 °C decreased obviously, indicating that the single rutile TNTs has low catalytic activity and is lower than that of single anatase. From the photocatalytic degradation rate chart in Figure 7i, it can be seen that the degradation rates from high to low are 600 °C > 500 °C > 300 °C > 400 °C > uncalcined > blank. The degradation rate of TNTs calcined at 600 °C can reach 0.0186 min⁻¹, which is four times that of uncalcined TNTs (0.00472 min⁻¹). The degradation rate can also indicate that TNTs with a certain proportion of anatase and rutile have the highest activity. Compared with the TiO₂ materials prepared in other articles, although the degradation rate of the TiO₂ nanotubes prepared in this article is not the best, it has surpassed some modified TiO₂ nanomaterials and far exceeds that of pure TiO₂ (P25) as shown in Table I. The standard error of Figure7(i) is calculated as shown in Table II, and all errors are within the acceptable range.

Cycle performance and catalytic mechanism

For photocatalytic materials, high catalytic efficiency and high stability are required, which can be reused without losing activity. Therefore, TNTs calcined at 600 °C were recycled and tested for stability. The sample was catalyzed six times and the final degradation rate was recorded each time (Figure 8a and Table III). It can be seen that after six cycles of use, the final catalytic effect of the sample did not obviously decrease. This shows that TNTs are stable and can be reused without losing activity. As shown in Figure 8b and Table IV, the photocatalytic activity did not decrease significantly after the addition of p-benzoquinone (BQ) to the TNTs system. The addition of tert-butanol (TBA) and triethanolamine (TEOA) significantly reduced the degradation rate, indicating that h⁺ and ·OH are the main active substances. The standard error calculation of each catalytic result shows that it is within the allowable range of error.

In order to further reveal the photocatalytic mechanism of TNTs, the following formulas are

Table I. Some TiO₂ materials and degradation rate table.

Sample	Ag-TiO ₂ [Liu et al. 2020]	AgI/TiO ₂ [Li et al. 2008]	TiO ₂ NTA/Ag-AgBr [Cao et al. 2019]	TiO ₂ (P25)[Xiao et al. 2018]
Degradation rate/ min ⁻¹	0.0052	0.011	0.025	0.000139

Table II. Standard error table of all samples.

Samples	Intercept		Slope	
	Value	Standard error	Value	Standard error
300°CTNTs	-0.09874	0.06238	0.00585	6.55124×10 ⁻⁴
400°CTNTs	0.14441	0.03619	0.00536	3.58338×10 ⁻⁴
500°CTNTs	-0.22808	0.11252	0.01679	0.00118
600°CTNTs	-0.09978	0.12071	0.0184	0.00127
700°CTNTs	-0.01189	0.02554	0.00436	2.68182×10 ⁻⁴
Uncalcined	0.04345	0.02695	0.00472	2.83033×10 ⁻⁴
Blank	0.01574	0.00781	4.9471×10 ⁻⁴	8.20603×10 ⁻⁵

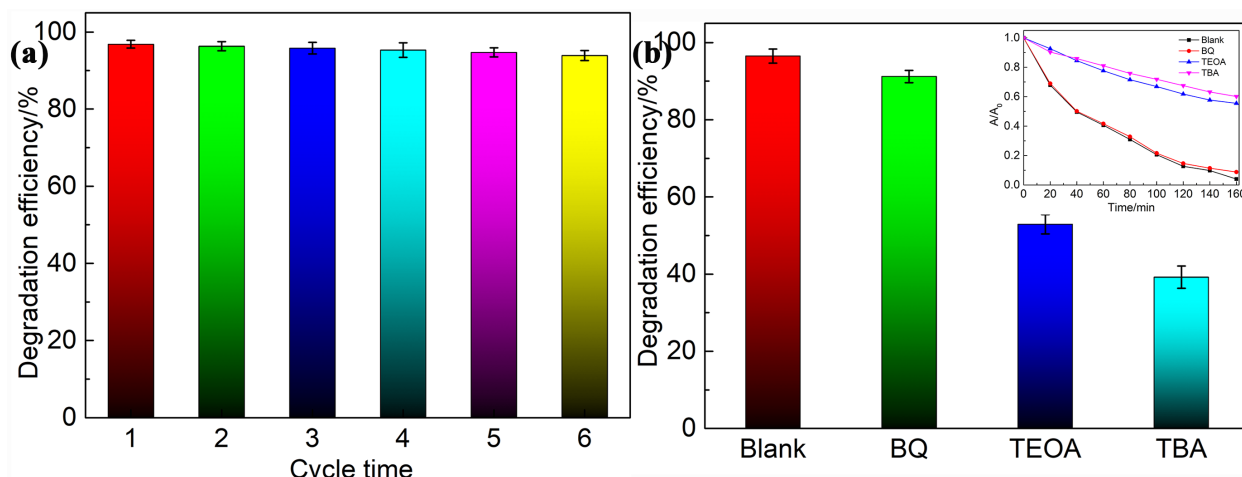


Figure 8. (a) Photocatalytic cycle performance of TNTs calcined at 600 °C and (b). reactant capture diagram.

used to calculate the valence and conduction band values (Tonda et al. 2015).

$$E_{CB} = X - E^e - \frac{E_g}{2}$$

$$E_{VB} = E_{CB} + E_g$$

X is absolute electronegativity, and the X value of TiO₂ is 5.8 eV (Chen et al. 2014). E^e is a constant relative to the standard H electrode (E^e value is 4.5 eV), E_g is the band gap (Chen et al. 2014, Huang et al. 2016). E_{VB} values of TNTs were calculated to be 2.69 eV, and E_{CB} values were -0.09 eV. The potential of the valence band edge (2.69 eV) is more positive than the oxidation potentials of OH⁻/·OH (1.99 eV) and H₂O/·OH (2.34 eV). Thus, the photogenerated holes of TNTs can react with OH⁻ or H₂O to generate ·OH. The potential of O₂/·O₂⁻ is -0.33 eV, which is lower than the E_{CB} value of TiO₂ nanotubes, so O₂ cannot be reduced to ·O₂⁻, and ·O₂⁻ is not an active species in the system. Therefore, only h⁺ and ·O₂⁻ can play a role in the catalytic process, and a redox reaction occurs with the pollutants, thereby achieving the effect of degrading the pollutants. TNTs containing both anatase and rutile can effectively improve the separation of photogenerated electron-hole pairs, greatly reduce the possibility of charge recombination,

and thus improve the photocatalytic activity of the material. From the above PL, photocurrent and catalytic properties, it can be seen that the recombination of electron-hole pairs is suppressed, and the direct oxidation ability of holes is greatly improved, so that h⁺ and ·OH become active species in TNTs. Figure 9 shows the mechanism of catalytic degradation of RhB. The specific process of catalytic degradation of RhB by TNTs as follows:

Table III. Standard error table of cycle performance test.

Cycle times	Average value	Standard error
1	0.966	0.00728
2	0.960	0.00839
3	0.958	0.00947
4	0.952	0.0104
5	0.949	0.00749
6	0.943	0.00802

Table IV. Standard error table of mechanism test.

Scavengers	Average value	Standard error
Blank	0.965	0.00973
BQ	0.912	0.00986
TEOA	0.529	0.01120
TBA	0.392	0.01324

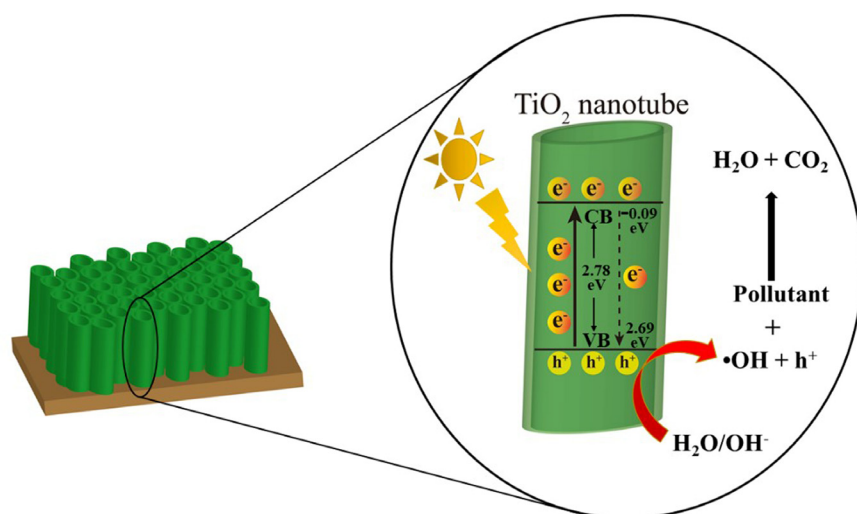


Figure 9. Catalytic mechanism diagram of TNTs.

CONCLUSIONS

TiO₂ nanotubes are prepared by anodization, and samples with different crystal phases can be obtained by calcination. The TiO₂ nanotubes calcined at 600 °C contained two phases of anatase and rutile, and showed the highest RhB degradation rate under visible light. The final catalytic efficiency can reach 96%. This is because the combination of the anatase and rutile phases reduces the charge transfer resistance and effectively inhibits the recombination of electron-hole pairs, thereby improving the photocatalytic activity. At the same time, cyclic tests show that the prepared catalyst has good stability and can be reused many times, so it has broad application prospects in solving environmental pollution.

Acknowledgments

This work was supported by the Natural Science Foundation of Shandong Province of China (No. ZR2019MEM020, No. ZR2017LEM004), the Fundamental Research Funds for the Central Universities of China (No. 18CX02091A) and the Open Fund (No. OGE201702-07) of Key Laboratory of Oil & Gas Equipment, Ministry of Education (Southwest Petroleum University).

REFERENCES

- ADAWIYA J, HAIDER H & RIYAD. 2017. Exploring potential environmental applications of TiO₂ nanoparticles. *Energy Procedia* 119: 332-345. doi: 10.1016/j.egypro.2017.07.117.
- BARNARD AS & CURTISS LA. 2005. Prediction of TiO₂ nanoparticle phase and shape transitions controlled by surface chemistry. *Nano Lett* 5: 1261-1266. doi: doi.org/10.1021/nl050355m.
- BICKLEY IB, GONZALEZ-CARRENO T & LEES JS. 1991. A structural investigation of titanium dioxide photocatalysts. *J Solid State Chem* 92: 178-190. doi: 10.1016/0022-4596(91)90255-G.
- CAO DD, WANG QY, LIU ZY, ZHANG H, WANG YJ, JIN RC & GAO SM. 2019. Enhanced the photoelectrocatalytic performance of TiO₂ nanotube arrays by the synergistic sensitization of AgAgBr nanospheres. *Spectrochim Acta A* 227: 1386-1425. doi:10.1016/j.saa.2019.117674.
- CHEN S, HU Y, MENG S & FU X. 2014. Study on the separation mechanisms of photogenerated electrons and holes for composite photocatalysts g-C₃N₄-WO₃. *Appl Catal B-Environ* 150-151: 564-573. doi: 10.1016/j.apcatb.2013.12.053.
- CHIARELLO GL, ROSSETTI I & FORNI L. 2005. Flame-spray pyrolysis preparation of perovskites for methane catalytic combustion. *J Catal* 236: 251-261. doi: 10.1016/j.jcat.2005.10.003.
- CHOI Y, KIM H, MOON G, JO SG & CHOI WY. 2016. Boosting up the low catalytic activity of silver for H₂ production on Ag/TiO₂ photocatalyst: thiocyanate as a selective modifier. *ACS Publications* 6: 821-828. doi: 10.1021/acscatal.5b02376.

- DICESARE N & LAKOWICZ JR. 2001. Spectral properties of fluoro-phores combining the boronic acid group with electron do-nor or withdrawing groups. Implication in the development of fluorescence probed for saccharides. *J Phys Chem A* 105: 6834-6840.
- DUY NV, HIEU NV, HUY PT, CHIEN ND & THAMILSELVAN M. 2008. Mixed SnO₂/TiO₂ included with carbon nanotubes for gas-sensing application. *Physica E* 41: 258-263. doi: 10.1016/j.physe.2008.07.007.
- FENG CY, DENG YC, TANG L, ZENG GM & WANG JJ. 2018. Core-shell Ag₂CrO₄/N-GQDs@g-C₃N₄ composites with anti-photocorrosion performance for enhanced full-spectrum-light photocatalytic activities. *Appl Catal B: Environ* 239: 525-536. doi: 10.1016/j.apcatb.2018.08.049.
- FITRA M, DAUT I, IRWANTO M, GOMESH N & IRWAN YM. 2013. Effect of TiO₂ thickness dye solar cell on charge generation. *Energy Procedia* 36: 278-286. doi: 10.1016/j.egypro.2013.07.032.
- GAO SW, LAN Z, WU WX, QUE LF & WU JH. 2014. Fabrication and photovoltaic performance of high efficiency front-illuminated dye-sensitized solar cell based on ordered TiO₂ nanotube arrays. *Acta Phys Chim Sin* (3): 446-452. doi: 10.3866/PKU.WHXB201401022.
- GHAYEB MMY & GHONCHEGI Z. 2015. Fabrication and characterization of copper doped TiO₂ nanotube arrays by in situ electrochemical method as efficient visible-light photocatalyst. *Ceram Int* 41: 8735-8741. doi: 10.1016/j.ceramint.2015.03.094.
- HONG Y, LI C, ZHANG G, MENG Y & YIN. 2016. Efficient and stable Nb₂O₅ modified g-C₃N₄ photocatalyst for removal of antibiotic pollutant. *Chem Eng J* 299: 74-84. doi: 10.1016/j.jece.2015.03.021.
- HUANG K, LIU C, YAN X, HUANG CY & CHEN JB. 2016. Hydrothermal synthesis of g-C₃N₄/CdWO₄ nanocomposite and enhanced photocatalytic activity for tetracycline degradation under visible light. *Crystengcomm* 18: 6453-6463. doi: 10.1016/j.seppur.2017.07.026.
- HWANG KJ, LEE JW, YOO SJ, JEONG SY & JEONG DH. 2013. Fine size-regulation of nanocrystalline anatase-TiO₂ via sol-gel synthesis and subsequent phase transformation by calcination. *New J Chem* 37: 1378-1384. doi: 10.1039/C3NJ41170B.
- LI H, WU X, YIN S, KATSUMATA K & WANG YH. 2017. Effect of rutile TiO₂ on the photocatalytic performance of g-C₃N₄/brookite-TiO₂-xNy photocatalyst for NO decomposition. *Appl Surf Sci* 392: 531-539. doi: 10.1016/j.apsusc.2016.09.075.
- LI R, LI Q, ZONG L, WANG XD, YANG JJ. 2013. BaTiO₃/TiO₂ heterostructure nanotube arrays for improved photoelectrochemical and photocatalytic activity. *Electrochim Acta* 91: 30-35. doi: 10.1016/j.electacta.2012.12.073.
- LI YZ, ZHANG H, GUO ZM, HAN JJ, ZHAO XJ, ZHAO QG & KIM SJ. 2008. Highly efficient visible-light-induced photocatalytic activity of nanostructured AgI/TiO₂ photocatalyst. *Langmuir* 24: 8351-8357. doi:10.1021/la801046u.
- LIANG YC, WANG CC, KEI CC, HSUEH YC & CHO WH. 2011. Photocatalysis of Ag-loaded TiO₂ nanotube arrays formed by atomic layer deposition. *J Physica Chem C* 115: 9498-9502. doi: 10.1021/cg301230w.
- LIU J, LI Y & ARUMUGAM S. 2018. Investigation of low temperature processed titanium dioxide (TiO₂) films for printed dye sensitized solar cells (DSSCs) for large area flexible applications. *Mater Today Commun* 5: 13846-13854. doi: 10.1016/j.matpr.2018.02.026.
- LIU R, WANG P, WANG XF, YU HG & YU JG. 2020. UV- and visible-light photocatalytic activity of simultaneously deposited and doped Ag/Ag(I)-TiO₂ photocatalyst. *J Phys Chem C* 14: 16-22. doi:10.1021/jp305774n.
- LUO J, ZHOU XS, MA L & XU Y. 2015. Enhancing visible-light photocatalytic activity of g-C₃N₄ by doping phosphorus and coupling with CeO₂ for the degradation of methyl orange under visible light irradiation. *RSC Adv* 5: 568728-68735. doi: 10.1039/C5RA10848A.
- MACAK JM, ZLAMAL M, KRYSAJ & SCHMUKI P. 2007. Self-organized TiO₂ nanotube layers as highly efficient photocatalysts. *small* 3: 300-304. doi: 10.1002/sml.200600426.
- MAMAKHEL A, TYRSTED C, JESEN ED, HALD P & IVERSEN BB. 2013. Direct formation of crystalline phase pure rutile TiO₂ nanostructures by a facile hydrothermal method. *Cryst Growth Des* 13: 4730-4734. doi: 10.1021/cg400858p.
- MI JL, CLAUSEN C & BREMHOLM M. 2012. Rapid hydrothermal preparation of rutile TiO₂ nanoparticles by simultaneous transformation of primary brookite and anatase: An in situ synchrotron PXRD study. *Cryst Growth Des* 1: 6092-6097. doi: 10.1016/j.cej.2016.04.092.
- MOHAMED AER & ROHANI S. 2011. Modified TiO₂ nanotube arrays (TNATs): progressive strategies towards visible light responsive photoanode, a review. *Energy Environ Sci* 4: 1065-1086. doi: 10.1039/C0EE00488J.
- MORRIS D, EGDELL RG & MATER J. 2001. Application of V-doped TiO₂ as a sensor for detection of SO₂. *Chem* 11: 3207-3210. doi: 10.1039/B104801P.
- PHAM TD, LEE BK, LEE CH & RHEUMATOL BJ. 2016. The advanced removal of benzene from aerosols by photocatalytic oxidation and adsorption of Cu-TiO₂/PU under visible

light irradiation. *Appl Catal B: Environ* 36: 1341-1342. doi: 10.1016/j.apcatb.2015.09.023.

QAMAR M, DRMOSH Q, AHMED MI, QAMARUDDIN M & YAMANI ZH. 2015. Enhanced photoelectrochemical and photocatalytic activity of WO₃-surface modified TiO₂ thin film. *Nanoscale Res Lett* 10: 54. doi: 10.1186/s11671-015-0745-2.

QIAN X, HAN H, CHEN Y & YUAN Y. 2018. Sol-gel solvothermal route to synthesize anatase/brookite /rutile TiO₂ nanocomposites with highly photocatalytic activity. *J Sol-Gel Sci Technol* 85: 394-401. doi: 10.1007/s10971-017-4544-3.

SUGIMOTO T, ZHOU X & MURAMATSU A. 2002. Synthesis of Uniform anatase TiO₂ nanoparticles by gel-sol method: 1. solution chemistry of Ti(OH)ⁿ⁽⁴⁻ⁿ⁾⁺ complexes. *J. Colloid. Inter Sci* 252: 339-346. doi: 10.1006/jcis.2002.8454.

SUN H, GUI Y, WEI H, LONG YK, WANG Q & TANG C. 2019. DFT study of SF₆ decomposed products on Pd-TiO₂: gas sensing mechanism study. *Adsorption* 25: 1643-1653. doi: 10.1007/s10450-019-00150-1.

TIAN H, MA J, LI K & LI JJ. 2009. Hydrothermal synthesis of S-doped TiO₂ nanoparticles and their photocatalytic ability for degradation of methyl orange. *Ceram Int* 35: 1289-1292. doi: 10.1016/j.ceramint.2008.05.003.

TIENG S, KANAIEV A & CHHOR K. 2011. New homogeneously doped Fe(III)-TiO₂ photocatalyst for gaseous pollutant degradation. *Appl Catal A: Gen* 399: 191-197. doi: 10.1016/j.apcata.2011.03.056.

TONDA S, KUMAR S & SHANKER V. 2015. In situ growth strategy for highly efficient Ag₂CO₃/g-C₃N₄ hetero/nanojunctions with enhanced photocatalytic activity under sunlight irradiation. *J Environ Chem Eng* 3: 852-861. doi: 10.1016/j.jece.2015.03.021.

WANG Y, FANG HB, ZHENG YZ, YE R & TAO X. 2015. Controllable assembly of well-defined monodisperse Au nanoparticles on hierarchical ZnO microspheres for enhanced visible-light-driven photocatalytic and antibacterial activity. *Nanoscale* 7: 19118-19128. doi: 10.1039/C5NR06359K.

WILEY JP, HUGHES KA, KAISER RJ, KESICKI EA & LI GS. 2001. Phenylboronic acid salicylhydroxamic acid bioconjugates 2 polyvalent im-mobilization of protein ligands for affinity chromatography. *Bioconjugate Chem* 12: 240-250. doi: 10.1021/bc0000942.

WU J, FENG YJ, LOGAN BE, DAI CC & HAN XY. 2019. Preparation of Al-O-linked porous-g-C₃N₄/TiO₂-nanotube Z-Scheme composites for efficient photocatalytic CO₂ conversion and 2,4-dichlorophenol decomposition and mechanism. *ACS Sustainable Chem Eng* 7: 15289-15296. doi: 10.1021/acssuschemeng.9b02489.

XIAO JQ, LIN KS & YU Y. 2018. Novel Ag@AgCl@AgBr heterostructured nanotubes as high-performance visible-light photocatalysts for decomposition of dyes. *Catal today* 314: 10-19. doi:10.1016/j.cattod.2018.04.019.

ZENG M, LI Y, MAO M, BAI L & REN L. 2015. Synergetic effect between photocatalysis on TiO₂ and thermocatalysis on CeO₂ for gas-phase oxidation of benzene on TiO₂/CeO₂ nanocomposites. *ACS Catal* 5: 3278-3286. doi: 10.1021/acscatal.5b00292.

ZHANG DQ, LI GS & YANG XF. 2009. A micrometer-size TiO₂ single-crystal photocatalyst with remarkable 80% level of reactive facets. *Chem Commun* 29: 4381-4383. doi: 10.1021/cg400858p.

ZHANG M, LU D, ZHANG Z, GUO Y & YANG J. 2015. Enhanced photocurrent and photocatalytic degradation of methyl orange by VN codoped TiO₂ nanotube arrays cooperated with H₂O₂. *J Electrochem Soc* 162: 557-563. doi: 10.1149/2.0901508jes.

How to cite

LIU E & BI X. 2023. TiO₂ nanotube arrays with visible light catalytic. *An Acad Bras Cienc* 95: e20201164. DOI 10.1590/0001-37652023020201164.

*Manuscript received on July 22, 2020;
accepted for publication on October 9, 2020*

ENYANG LIU¹

<https://orcid.org/0000-0002-2448-5175>

XIAOJIAN BI²

<https://orcid.org/0000-0003-4141-5467>

¹School of Materials Science and Engineering, China University of Petroleum (East China), Qingdao 266580, China

²Offshore Oil Engineering Co. Ltd, Tianjin 300451, China

Correspondence to: **Enyang Liu**

E-mail: enyangliu@126.com

Author contribution

Xiaojian Bi: Conceptualization, Methodology, Software, Investigation, Writing-original draft, Project administration;

EnyangLiu: Conceptualization, Methodology, Software, Investigation, Writing-review & editing.

